Loss Optimization of MMC by Second-Order Harmonic Circulating Current Injection

Limin Yang, Yaohua Li, Zixin Li, *Senior Member, IEEE*, Ping Wang, Shukai Xu, and Ruifeng Gou

***Abstract*—For high power voltage source converter based high voltage direct current transmission systems, modular multilevel converter (MMC) is the most popular circuit topology nowadays. It is known that the existence of the second-order harmonic circulating current (SHCC) component in the arm current of MMC increases the loss of the converter. Conventionally, the SHCC component eliminating methods are usually adopted to reduce the loss. The relationship between the loss of MMC and the SHCC component is analyzed first in this paper. The analysis shows that the conventional eliminating methods are not optimal in terms of the minimum loss of MMC. A loss optimization control scheme is also proposed by injecting the optimal SHCC component into the arm current of MMC, rather than eliminating the SHCC component of the arm current. The simulation and experimental results of the ±350 kV/1000 MW MMC and the down-scaled MMC setup verify the correctness and effectiveness of the proposed loss optimization method under different operation conditions.**

***Index Terms*—Circulating current injection, loss optimization, modular multilevel converter (MMC).**

I. Introduction

MODULAR multilevel converter (MMC) was first presented by Prof. R. Marquardt [1], which is a promising topology for the voltage source converter based high voltage direct current (VSC-HVdc) transmission systems. Compared to the line commutated converter, two-level and three-level converters, MMC has the characteristics of low harmonics, scalability, and high reliability [2]–[5]. Hence, it has been widely adopted in the applications of the integration of renewable resources and the connections of asynchronous ac networks [6].

The schematic of MMC is presented in Fig. 1. It consists of six arms. Each arm of the MMC has a total of N submodules (SMs) and one inductor L_0. Every SM includes one capacitor, two insulated gate bipolar translators (IGBTs) and two diodes. The large amount of IGBTs and diodes produce great loss in MMC, which mainly includes the conduction loss ($P_{\rm conT}$, $P_{\rm conD}$) of the IGBTs and diodes, IGBT switching loss ($E_{\rm sw}$), and the reverse recovery loss ($E_{\rm rec}$) of the diodes. The $P_{\rm conT}$ and $P_{\rm conD}$ are determined by the arm current flowing through the IGBTs and diodes in SMs, and the $E_{\rm sw}$ and $E_{\rm rec}$ are influenced by the average switching frequency and the switching current [7]. Because of the sorting-based SM voltage balancing control method, a single SM has a complex switching pattern [8]. It imposes great challenge on the research of the loss characteristics of MMC. The simulation look-up table method is widely used and accepted in studying the loss when MMC works under definite operation conditions [9]–[11]. But, it cannot reveal the mathematical relationship between the loss and the two variables, the arm current, and the average switching frequency of MMC clearly. The loss analytical methods were proposed in [12]–[14], which show the positive correlation relationship between the loss of MMC and the RMS value of the arm current. Zygmanowski *et al.* [12] and Qiang *et al.* [14] also present that the $E_{\rm sw}$ and $E_{\rm rec}$ increase with the average switching frequency.

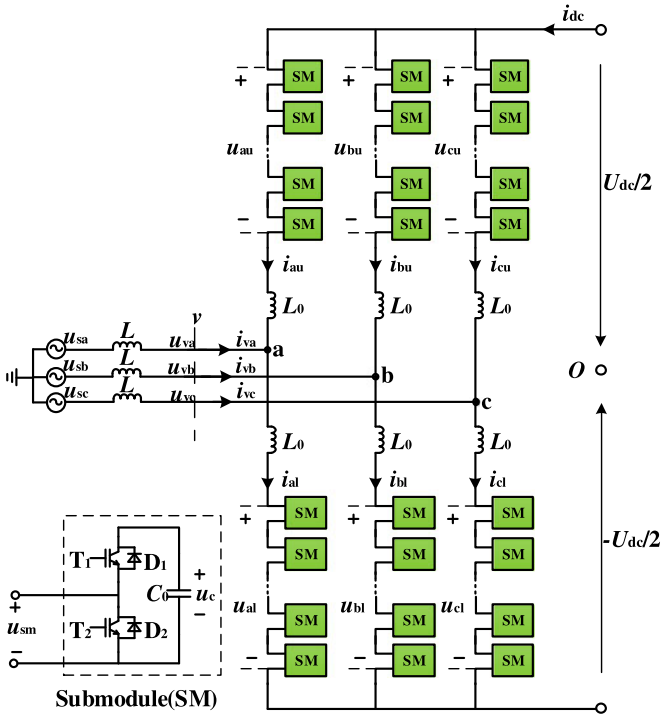

Fig. 1. Circuit topology of MMC.

Manuscript received March 13, 2017; revised June 22, 2017; accepted September 2, 2017. Date of publication September 10, 2017; date of current version March 5, 2018. This work was supported by the National High-Tech R&D Program of China (863 Program) under Grant 2015AA050102. Recommended for publication by Associate Editor M. Hagiwara. *(Corresponding author: Limin Yang.)*

L. Yang, Y. Li, Z. Li, and P. Wang are with the Key Laboratory of Power Electronics and Electric Drive, Institute of Electrical Engineering, Chinese Academy of Sciences, Beijing 100190, China, and also with the University of Chinese Academy of Sciences, Beijing 100049, China (e-mail: yanglimin@mail.iee.ac.cn; yhli@mail.iee.ac.cn; lzx@mail.iee.ac.cn; wangping@mail.iee.ac.cn).

S. Xu is with the China Southern Power Grid Company, Ltd., Guangzhou 510530, China (e-mail: xusk@csg.cn).

R. Gou is with the Xi'an XD Power Systems Company, Ltd., Xi'an 710065, China (e-mail: gourf@xdps.com.cn).

Color versions of one or more of the figures in this paper are available online at http://ieeexplore.ieee.org.

Digital Object Identifier 10.1109/TPEL.2017.2751068

Reduction of the average switching frequency is one kind of the methods to optimize the loss of MMC. The average switching frequency consists of two parts: the switching frequency for modulation and for SM voltage balancing [15], [16]. The switching frequency for modulation is constant when MMC operates under definite operation conditions. The switching frequency for SM voltage balancing is influenced by the balancing methods, which mainly include the methods based on pulse width modulation (PWM) [17], [18] and nearest level modulation (NLM) [8], [19]–[22]. The SMs switch ON and OFF in every control cycle with the voltage balancing strategies based on the level-shifted PWM [17] and the phase-shifted PWM [18]. The high switching frequency of PWM brings a lot of switching loss. So, these kind of methods are not suitable for the MMC with large numbers of SMs. The reduced switching frequency (RSF) voltage balancing strategy based on NLM to reduce the switching loss is present in [19]–[21]. The RSF strategy reduces the switching frequency at the cost of the large fluctuation of the SMs' voltage. Thus, the RSF methods may threaten the safe operation of SMs when the load is heavy. Qin [22] proposed a method to reduce the switching frequency in which an SM voltage band value was set. But it is hard to determine the relationship between the switching frequency and the band value. Li *et al*. [8] present a low switching frequency (LSF) voltage balancing method, which introduces the balancing adjusting SM number $N_{\rm ban}$. In every control cycle, the number of SMs switched ON or OFF is fixed to $N_{\rm ban}$ for voltage balancing. In comparison with the RSF methods, the ripple of SMs' capacitor voltage can be reduced and the average switching frequency of SMs can also be evaluated accurately by using the LSF voltage balancing method.

Optimization of the arm current is the other kind of methods to reduce the loss of MMC. The arm current of MMC mainly consists of the direct current component, the fundamental component, and the second-order harmonic circulating current (SHCC) component. There are fixed values of the direct current component and fundamental component in the arm current under definite operation conditions of MMC. The SHCC component is the only degree of freedom to reduce the loss of MMC through optimizing the arm current. Studies have been conducted on the relationship between the loss of MMC and the SHCC component by using the simulation look-up table method in [23] and [24], which point out that the loss can be reduced by eliminating the SHCC component. Thus, the conventional methods are presented in [19] and [25] to reduce the loss by eliminating the SHCC component. Tu *et al*. [19] proposed a closed-loop method based on proportional integral controller to eliminate the SHCC component in rotating frame. This method is suitable for the three-phase MMC under balanced conditions. Li *et al.* [25] introduced a control strategy based on paralleled proportional-resonant (PR) controller to eliminate the SHCC component. It is implemented in the stationary frame and can be applied to both single-phase and three-phase topologies. Yang *et al.* [26] revealed the relationship between the loss of MMC and the SHCC component as an inverter. The optimal SHCC component is injected to the arm current to increase the efficiency of MMC as an inverter. The SHCC injection method has also been mentioned in [27]. However, the SHCC injection method is used for mitigating the voltage fluctuation of SMs in this paper and it is not mentioned to inject the optimal SHCC component to minimize the loss of MMC.

According to the analysis of the aforementioned strategies to reduce the loss of MMC, it is known that a deep study has been carried out on the loss optimization schemes based on reducing the average switching frequency, while it is still necessary to make more efforts in the loss optimization methods of injecting the optimal SHCC component. This paper presents the relationship between the loss of MMC and the amplitude and phase of the SHCC component first based on the LSF voltage balancing method [8]. The optimal amplitude and phase of the SHCC component are derived under the condition that MMC operates as an inverter and a rectifier, respectively. Then, the loss optimization control strategy based on SHCC injection is proposed. The effectiveness of the proposed loss optimization method is verified by the computer simulation results based on the time-domain simulation tool PSCAD/EMTDC, the real-time hardware in the loop (HIL) test results, and the experimental results on $\pm$350 kV/1000 MW MMC in the Luxi Back-to-Back DC Asynchronous Networking Project [28]. Additionally, the correctness of the proposed method is verified on a down-scaled 200 V/3.8 kW MMC setup.

This paper is organized as follows. The relationship between the loss of MMC and the SHCC component is derived based on the loss analytical methods proposed by [13] in Section II. In Section III, the loss optimization scheme based on SHCC injection is depicted. The $\pm$350 kV/1000 MW PSCAD/EMTDC simulation results of the proposed control method are presented in Section IV. In Section V, the HIL test results and experimental results at the project site and on a down-scaled MMC setup are provided. Finally, the conclusions are drawn in Section VI.

II. Loss of MMC and the Optimal SHCC Component

A. Loss of MMC

The loss of MMC studied in this paper mainly refers to the SMs' loss produced by the IGBTs and diodes in the SMs, which include the conduction loss ($P_{\rm conT}$, $P_{\rm conD}$) of the IGBTs and diodes, IGBT switching loss ($E_{\rm on}$, $E_{\rm off}$), and the reverse recovery loss ($E_{\rm rec}$) of the diodes. The conduction characteristics of single IGBT and diode are expressed as (1) by linear fitting from the datasheet offered by the semiconductor device manufacturer. Here, $k_1 - k_4$ are the linear fitting coefficients, $V_{\rm ce}$ and V_F are the forward voltage drop of the IGBT and diode, and $I_{\rm c}$ is the conduction current

$$\begin{cases} V_{\rm ce} = k_1 I_c + k_2 \\ V_F = k_3 I_c + k_4 \end{cases}. \tag{1}$$

The upper and lower arms of phase A are named as arm AU and AL. Similarly, the upper and lower arms of phase B and C are named as arm BU, BL, CU and CL respectively. Take the arm AU for example, the conduction current $I_{\rm c}$ is equal to the absolute value of the arm current $|i_{\rm au}(t)|$. Thereby, the conduction loss $p_{\rm conIGBT}$, $p_{\rm conDiode}$ of IGBT and diode devices

can be calculated by

$$\begin{cases} p_{\mathrm{conIGBT}} = f_{\mathrm{conT}}\left(|i_{\mathrm{au}}(t)|\right) = k_1|i_{\mathrm{au}}(t)|^2 + k_2\,|i_{\mathrm{au}}(t)| \\ p_{\mathrm{conDiode}} = f_{\mathrm{conD}}\left(|i_{\mathrm{au}}(t)|\right) = k_3|i_{\mathrm{au}}(t)|^2 + k_4\,|i_{\mathrm{au}}(t)| \end{cases}. \tag{2}$$

The turn-on loss e_{onIGBT}, turn-off loss e_{offIGBT} of the IGBT, and the reverse recovery loss e_{recDiode} of diode devices can be expressed by quadratic curve fitting relationship as (3), where $\lambda_1 - \lambda_9$ are the fitting coefficients of IGBT and diode devices

$$\begin{cases} e_{\mathrm{onIGBT}} = f_{\mathrm{on}}\left(|i_{\mathrm{au}}(t)|\right) = \lambda_1|i_{\mathrm{au}}(t)|^2 + \lambda_2\,|i_{\mathrm{au}}(t)| + \lambda_3 \\ e_{\mathrm{offIGBT}} = f_{\mathrm{off}}\left(|i_{\mathrm{au}}(t)|\right) = \lambda_4|i_{\mathrm{au}}(t)|^2 + \lambda_5\,|i_{\mathrm{au}}(t)| + \lambda_6 \\ e_{\mathrm{recDiode}} = f_{\mathrm{rec}}\left(|i_{\mathrm{au}}(t)|\right) = \lambda_7|i_{\mathrm{au}}(t)|^2 + \lambda_8\,|i_{\mathrm{au}}(t)| + \lambda_9 \end{cases}. \tag{3}$$

According to the LSF voltage balancing method [8], the total number of the switching SMs and the put-in SMs can be calculated in terms of the whole arm during every control period T_{c}. So, the total conduction loss P_{con} and the total switch loss P_{sw} of the MMC can be derived as (4) [13] by computing the integral of (2) and (3)

$$\begin{cases} P_{\mathrm{con}} = P_{\mathrm{conT}} + P_{\mathrm{conD}} = C_{\mathrm{con1}}I^2_{\mathrm{au\_RMS}} \\ \qquad +C_{\mathrm{con2}}I_{\mathrm{au\_absAVE}} + C_{\mathrm{con3}} \\ P_{\mathrm{sw}} = (E_{\mathrm{on}} + E_{\mathrm{off}} + E_{\mathrm{rec}})/T_f = C_{\mathrm{swTotal1}}I^2_{\mathrm{au\_RMS}} \\ \qquad +C_{\mathrm{swTotal2}}I_{\mathrm{au\_absAVE}} + C_{\mathrm{swTotal3}} \end{cases} \tag{4}$$

where T_f is the fundamental cycle; the nonnegative C_{con1}, C_{con2}, and C_{con3} are the coefficients of the conduction loss, which are the functions of the SM number *N*, active power *P*, modulation ratio *m*, system parameters and the fitting coefficients $k_1 - k_4$; the nonnegative C_{swTotal1}, C_{swTotal2}, and C_{swTotal3} are the coefficients of the switching loss, which are the functions of *N*, *m*, N_{ban}, the rated voltage U_{smN} of SMs, system parameters and the fitting coefficients $\lambda_1 - \lambda_9$; $I_{\mathrm{au\_RMS}}$ above is the RMS value of $i_{\mathrm{au}}(t)$; and $I_{\mathrm{au\_absAVE}}$ is the mean value of $|i_{\mathrm{au}}(t)|$.

When the MMC operates normally, the total loss is related to the arm current of MMC. According to the mean value theorem for integral, it can be easily proved that $I_{\mathrm{au\_RMS}} = \xi I_{\mathrm{au\_absAVE}}$, $\xi > 0$, and ξ is a variable depending on the MMC operation condition. Thus, the total loss P_{loss} of MMC can be calculated by

$$\begin{aligned} P_{\mathrm{loss}} = {} & \left(C_{\mathrm{con1}} + C_{\mathrm{swTotal1}}\right)\xi^2 I^2_{\mathrm{au\_absAVE}} + (C_{\mathrm{con2}} \\ & + C_{\mathrm{swTotal2}})I_{\mathrm{au\_absAVE}} + (C_{\mathrm{con3}} + C_{\mathrm{swTotal3}})\,. \end{aligned} \tag{5}$$

If the modulation method, voltage balancing method, and the operation condition of the MMC are determined, there is a positive correlation relationship between the loss of MMC and the $I_{\mathrm{au\_absAVE}}$.

The upper arm current of the phase A is described in Fig. 2 and expressed by $i_{\mathrm{au}}(t) = I_{\mathrm{dca}} + I_{\mathrm{m}}\sin(\omega t + \varphi) + I_{2\mathrm{m}}\sin(2\omega t + \delta)$. I_{dca} is the direct current component, I_{m} and φ are the amplitude and phase of the fundamental component, and $I_{2\mathrm{m}}$ and δ are the amplitude and phase of the SHCC component.

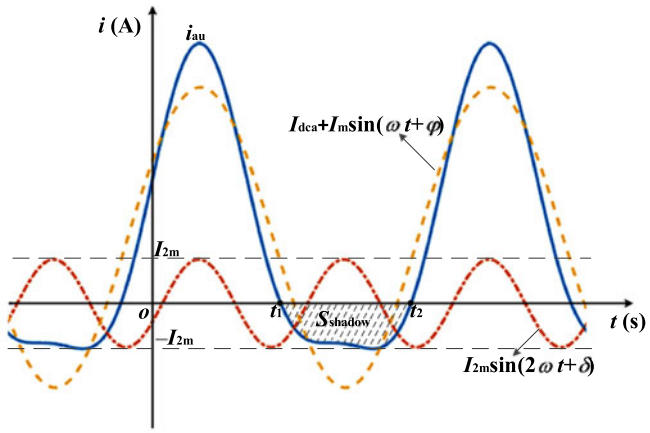

Fig. 2. Diagram of the arm current $i_{\mathrm{au}}(t)$.

The $I_{\mathrm{au\_absAVE}}$ can be calculated by

$$\begin{aligned} I_{\mathrm{au\_absAVE}} = {} & \frac{1}{T_f}\int_{t_1}^{t_1+T_f} |i_{\mathrm{au}}(t)|dt = I_{\mathrm{dca}} \\ & + \frac{2}{T_f}\int_{t_1}^{t_2} [-i_{\mathrm{au}}(t)]dt = I_{\mathrm{dca}} + S_{\mathrm{shadow}}. \end{aligned} \tag{6}$$

The t_1, t_2 above are the zero-crossing point of $i_{\mathrm{au}}(t)$. S_{shadow} is the negative area of $i_{\mathrm{au}}(t)$, as shown in Fig. 2. The conclusion can be drawn that there exists positive correlation relationship between the loss of MMC and the S_{shadow} from (5) and (6).

B. Optimal SHCC Component

As is known, if the output power of the MMC has been set, the values of I_{dca}, I_{m}, and φ are definite. Thereby, the minimum point of the S_{shadow}, that is the minimum loss of MMC, depends on the amplitude and the phase of the SHCC component. Substitute the expression of $i_{\mathrm{au}}(t)$ into (6), then S_{shadow} is derived as

$$\begin{aligned} S_{\mathrm{shadow}} = {} & \frac{2}{T}\int_{t_1}^{t_2} (-i_{\mathrm{au}}(t))dt = -\frac{2I_{\mathrm{dca}}}{T}(t_2 - t_1) \\ & + \frac{I_m}{\pi}\left[\cos(\omega t_2 + \varphi) - \cos(\omega t_1 + \varphi)\right] \\ & + \frac{I_{2m}}{2\pi}\left[\cos(2\omega t_2 + \delta) - \cos(2\omega t_1 + \delta)\right]. \end{aligned} \tag{7}$$

Due to the symmetry of the trigonometric function, it can be known that S_{shadow} is completely symmetric about the axes $\omega t = -\varphi + 5\pi/4$ when $\delta \in [2\varphi - 7\pi/2,\ 2\varphi - 5\pi/2]$ and $\delta \in [2\varphi - 5\pi/2,\ 2\varphi - 3\pi/2]$. So, take the interval of $\delta \in [2\varphi - 5\pi/2,\ 2\varphi - 3\pi/2]$ into consideration, when $i_{\mathrm{au}}(t) = 0$ and the MMC operates normally, the approximate root of t_1, t_2 can be calculated as follows.

1) $\delta \in \{2\varphi - 5\pi/2,\ 2\varphi - 5\pi/2 + 2\arcsin[(I_{2m} + I_{\rm dca})/I_m]\}$

$$\begin{cases} t_1 = -\frac{1}{\omega(q_1+q_2)}\left\{0.5q_2\left(\delta+\frac{\pi}{2}\right) + q_1\left[\varphi - \pi \right.\right. \\ \qquad \left.\left. +\arcsin\left(\frac{I_{2m}-I_{\rm dca}}{I_m}\right)\right] - 2I_{2m}\right\} \\ t_2 = -\frac{1}{\omega(q_1+q_2)}\left\{0.5q_2\left(\delta-\frac{\pi}{2}\right) + q_1\left[\varphi \right.\right. \\ \qquad \left.\left. +\arcsin\left(\frac{I_{2m}+I_{\rm dca}}{I_m}\right)\right] - 2I_{2m}\right\} \end{cases}. \quad (8)$$

2) $\delta \in \{2\varphi - 5\pi/2 + 2\arcsin[(I_{2m} + I_{\rm dca})/I_m,\ 2\varphi - 3\pi/2 + 2\arcsin[(I_{2m} - I_{\rm dca})/I_m]\}$

$$\begin{cases} t_1 = -\frac{1}{\omega(q_1+q_2)}\left\{0.5q_2\left(\delta+\frac{\pi}{2}\right) + q_1\left[\varphi - \pi \right.\right. \\ \qquad \left.\left. +\arcsin\left(\frac{I_{2m}-I_{\rm dca}}{I_m}\right)\right] - 2I_{2m}\right\} \\ t_2 = \frac{1}{\omega(q_1-q_2)}\left\{0.5q_2\left(\delta-\frac{3\pi}{2}\right) + q_1\left[\varphi \right.\right. \\ \qquad \left.\left. -\arcsin\left(\frac{I_{2m}+I_{\rm dca}}{I_m}\right)\right]\right\} \end{cases}. \quad (9)$$

3) $\delta \in \{2\varphi - 3\pi/2 + 2\arcsin[(I_{2\rm m} - I_{\rm dca})/I_{\rm m}], 2\varphi - 3\pi/2\}$

$$\begin{cases} t_1 = \frac{1}{\omega(q_1-q_2)}\left\{0.5q_2\left(\delta-\frac{\pi}{2}\right) - q_1\left[\varphi - \pi \right.\right. \\ \qquad \left.\left. +\arcsin\left(\frac{I_{2m}-I_{\rm dca}}{I_m}\right)\right]\right\} \\ t_2 = \frac{1}{\omega(q_1-q_2)}\left\{0.5q_2\left(\delta-\frac{3\pi}{2}\right) + q_1\left[\varphi \right.\right. \\ \qquad \left.\left. -\arcsin\left(\frac{I_{2m}+I_{\rm dca}}{I_m}\right)\right]\right\} \end{cases}. \quad (10)$$

In (8)–(10), the parameters q_1 and q_2 meet

$$\begin{cases} q_1 = \frac{2I_{2m}}{\arcsin\frac{I_{2m}-I_{\rm dca}}{I_m} + \arcsin\frac{I_{2m}+I_{\rm dca}}{I_m}} \\ q_2 = \frac{4I_{2m}}{\pi} \end{cases}. \quad (11)$$

According to (7)–(11), the derivative $dS_{\rm shadow}/d\delta$ can be calculated as an inverter and a rectifier, respectively. As an inverter, $I_{\rm dca} > 0$. And when $\delta \in [2\varphi - 7\pi/2,\ 2\varphi - 5\pi/2]$, $dS_{\rm shadow}/d\delta < 0$, i.e., the $S_{\rm shadow}$ decreases monotonically; when $\delta \in [2\varphi - 5\pi/2,\ 2\varphi - 3\pi/2]$, $dS_{\rm shadow}/d\delta > 0$, i.e., the $S_{\rm shadow}$ increases monotonically. So, if the MMC operates as an inverter, the $S_{\rm shadow}$ and the loss of MMC reach the minimum point at

$$\delta_{\rm Inv\,Min} = 2\varphi - \pi/2 \pm 2k\pi (k = 0, 1, 2, 3\ldots). \quad (12)$$

The $S_{\rm shadow}$ and the loss of MMC reach the maximum point at

$$\delta_{\rm InvMax} = 2\varphi + \pi/2 \pm 2k\pi (k = 0, 1, 2, 3\ldots). \quad (13)$$

As a rectifier, $I_{\rm dca} < 0$. And when $\delta \in [2\varphi - 7\pi/2,\ 2\varphi - 5\pi/2]$, $dS_{\rm shadow}/d\delta > 0$, i.e., the $S_{\rm shadow}$ increases monotonically; when $\delta \in [2\varphi - 5\pi/2,\ 2\varphi - 3\pi/2]$, $dS_{\rm shadow}/d\delta < 0$, i.e., the $S_{\rm shadow}$ decreases monotonically. So, if the MMC operates as a rectifier, the $S_{\rm shadow}$ and the loss of MMC reach the minimum point at

$$\delta_{\rm RecMin} = 2\varphi + \pi/2 \pm 2k\pi (k = 0, 1, 2, 3\ldots). \quad (14)$$

TABLE I
PARAMETERS OF THE MMC FOR SIMULATIONS AND EXPERIMENTS

Parameter	Value
Rated power, P [MW]	1000
AC output line to line voltage, U_s [kV]	375
AC equivalent inductance, L [mH]	0.25
DC voltage, $U_{\rm dc}$ [kV]	700
Number of SMs per arm, N	468
Rated number of redundant SMs, $N_{\rm fN}$	30
SM capacitance, C_0 [mF]	12
Arm inductance, L_0 [mH]	105
Rated SM capacitor voltage, $U_{\rm smN}$ [V]	1600
Balancing adjusting number, $N_{\rm ban}$	6
Control cycle, T_c [μs]	100

The $S_{\rm shadow}$ and the loss of MMC reach the maximum point at

$$\delta_{\rm RecMax} = 2\varphi - \pi/2 \pm 2k\pi (k = 0, 1, 2, 3\ldots). \quad (15)$$

Because of the symmetry of the optimal phase δ when MMC works as an inverter and a rectifier, the loss of MMC reaches the minimum point at the same value of the amplitude of the SHCC. Take the optimal phase δ as an inverter, for example, when δ is equal to $2\varphi - \pi/2 \pm 2k\pi\,(k = 0, 1, 2, 3\ldots)$, the arm current can be given as $i_{\rm au}(t) = I_{\rm dca} + I_m \sin(\omega t + \varphi) - I_{2m}[1 - 2\sin^2(\omega t + \varphi)]$. The root of $i_{\rm au}(t) = 0$ can be expressed as

$$\begin{cases} t_1 = -\frac{1}{\omega(q_1+q_2)}\left\{q_2\varphi - 2I_{2m}q_1\left[\varphi - \pi \right.\right. \\ \qquad \left.\left. +\arcsin\left(\frac{I_{2m}-I_{\rm dca}}{I_m}\right)\right]\right\} \\ t_2 = -\frac{1}{\omega(q_1+q_2)}\left\{q_2\left(\varphi-\frac{\pi}{2}\right) - 2I_{2m}q_1\left[\varphi \right.\right. \\ \qquad \left.\left. +\arcsin\left(\frac{I_{2m}+I_{\rm dca}}{I_m}\right)\right]\right\} \end{cases}. \quad (16)$$

The derivative $dS_{\rm shadow}/dI_{2m}$ can be derived from (7) and (16). When $dS_{\rm shadow}/dI_{2m} = 0$, the optimal I_{2m} can be calculated as (17) approximately

$$I_{2m\rm Min} = I_m \sin\left[1.2\sqrt{-\left(\arcsin\frac{I_{\rm dca}}{I_m}\right)^2 + 2.1\arcsin\frac{I_{\rm dca}}{I_m} + 1.35} - 0.09\arcsin\frac{I_{\rm dca}}{I_m} - 1.39\right]. \quad (17)$$

C. Verification of the Optimal SHCC Component

To prove the aforementioned analysis of the optimal phase and amplitude of the SHCC component, computer simulation is carried out first in the time-domain simulation software PSCAD/EMTDC. The loss of MMC is calculated by the simulation look-up table method [9], [11]. The MMC circuit is the same as that in Fig. 1. The simulation results are presented in Figs. 3–6 by using the parameters listed in Table I. The IGBT devices used in this paper are Infineon FZ1500R33HL3.

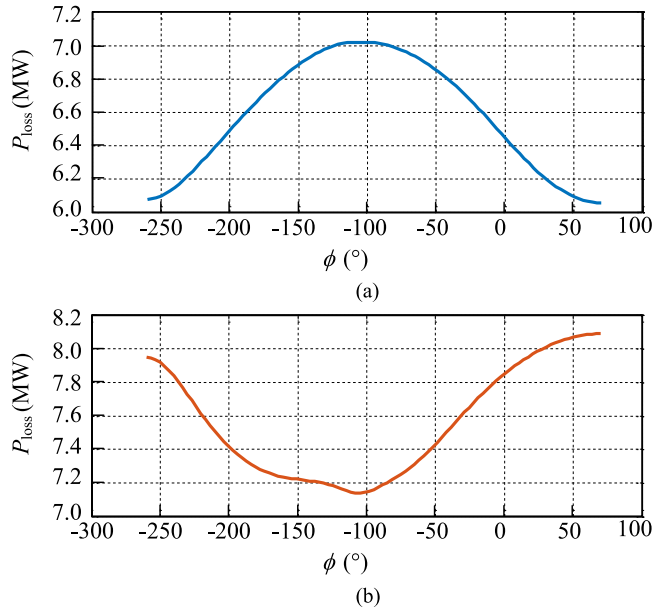

Fig. 3. Relationship between the loss of MMC and the phase of the SHCC component under rated 1000 MW. (a) Rectifier. (b) Inverter.

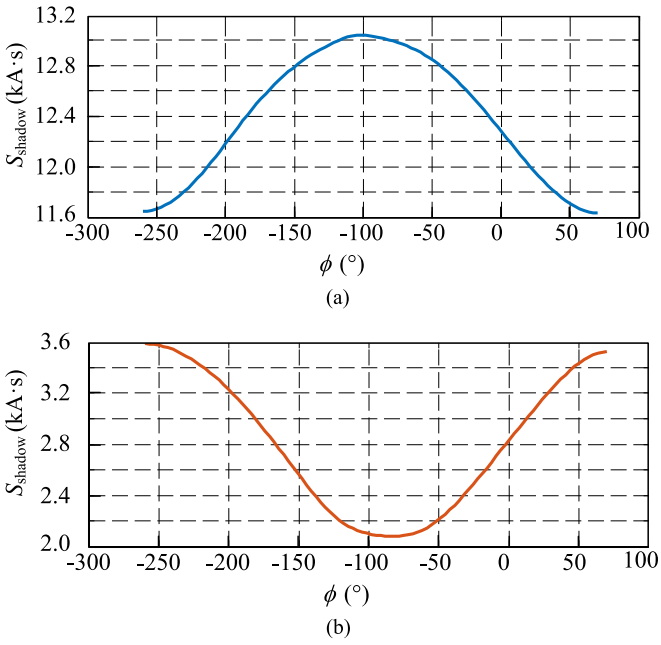

Fig. 4. Relationship between the S_{shadow} and the phase of the SHCC component under rated 1000 MW. (a) Rectifier. (b) Inverter.

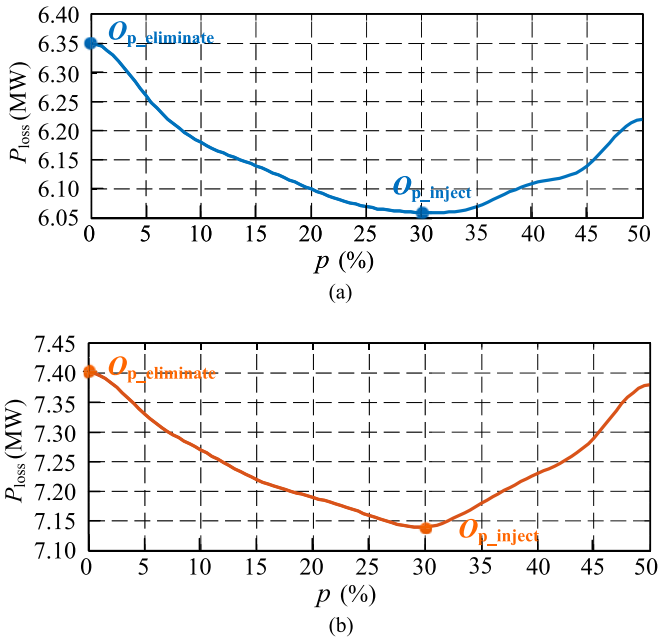

Fig. 5. Relationship between the loss of MMC and the amplitude of the SHCC component under rated 1000 MW. (a) Rectifier. (b) Inverter.

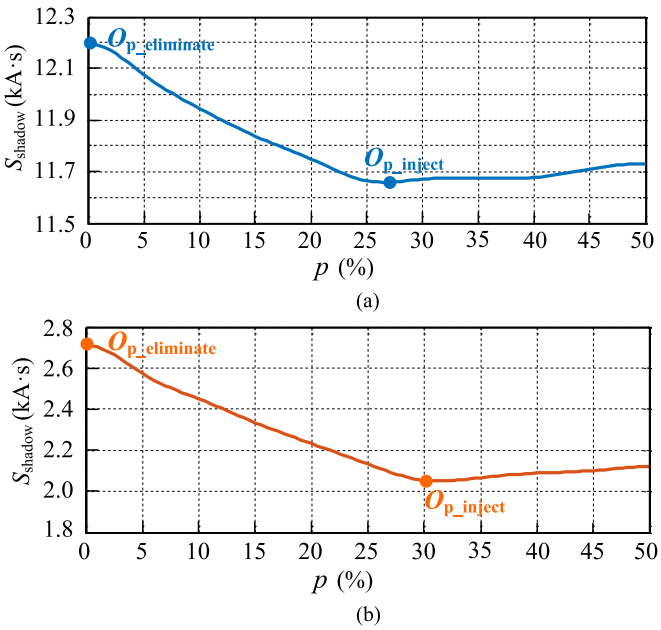

Fig. 6. Relationship between the S_{shadow} and the amplitude of the SHCC component under rated 1000 MW. (a) Rectifier. (b) Inverter.

Under the condition that the MMC operates as a rectifier under rated power 1000 MW, the loss of MMC can be calculated by the simulation look-up table method. If the percentage "p" of I_{2m} to I_m is kept at 30%, the relationship between the loss of MMC, the S_{shadow} of $i_{\mathrm{au}}(t)$, and the phase $\delta = \phi \cdot \pi/180^\circ$ of the SHCC component are shown as Figs. 3(a) and 4(a). If the phase δ of the SHCC component is set at the optimal point $\delta = 2\varphi + \pi/2$, the curves of the loss of MMC and the S_{shadow} of $i_{\mathrm{au}}(t)$ with different amplitudes, i.e., percentage "p," are given as Figs. 5(a) and 6(a).

Similarly, if the percentage "p" is kept at 30% under rated 1000 MW as an inverter, the loss of MMC and the S_{shadow} of $i_{\mathrm{au}}(t)$ under different phases $\delta = \phi \times \pi/180^\circ$ are shown as Figs. 3(b) and 4(b). If the phase δ is set to the optimal point $\delta = 2\varphi - \pi/2$ under rated 1000 MW as an inverter, the curves of the loss of MMC and the S_{shadow} of $i_{\mathrm{au}}(t)$ with different amplitudes are given as Figs. 5(b) and 6(b).

Take the phase of ac grid voltage as the reference value, the phase φ is measured in the simulation when the MMC operates under the rated power and unity power factor. The measured val-

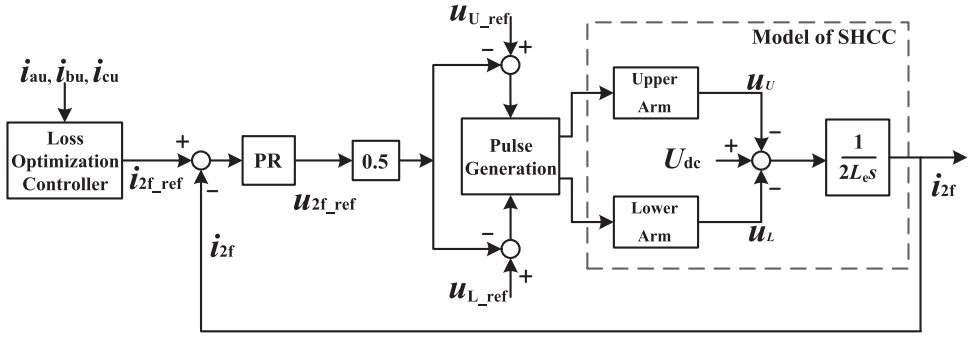

Fig. 7. Proposed loss optimization scheme based on the SHCC injection.

ues of the phase φ are equal to $0.7° \times \pi/180°$ as a rectifier and $-1.6° \times \pi/180°$ as an inverter. According to (12)–(15), the calculated values of the phase δ are given as follows. If $\delta_{\mathrm{RecMin}} = 2\varphi + \pi/2 = 2 \times 0.7° \times \pi/180° + \pi/2 = 0.508\pi$, i.e., $\phi_{\mathrm{RecMin}} = 91.4\,\mathrm{deg}$, the loss of MMC and S_{shadow} is minimum as a rectifier. If $\delta_{\mathrm{InvMin}} = 2\varphi - \pi/2 = 2 \times (-1.6°) \times \pi/180° - \pi/2 = -0.518\pi$, i.e., $\phi_{\mathrm{InvMin}} = -93.2\,\mathrm{deg}$, the loss of MMC and S_{shadow} is minimum as an inverter. Additionally, the loss of MMC and S_{shadow} reach the maximum point if $\delta_{\mathrm{RecMax}} = 2\varphi - \pi/2 = 2 \times 1.4° \times \pi/180° - \pi/2 = -0.492\pi$, i.e., $\phi_{\mathrm{RecMax}} = -88.6\,\mathrm{deg}$ as a rectifier and $\delta_{\mathrm{InvMax}} = 2\varphi + \pi/2 = 2 \times (-1.6°) \times \pi/180° + \pi/2 = 0.482\pi$, i.e., $\phi_{\mathrm{InvMax}} = 86.8\,\mathrm{deg}$ as an inverter. It is seen from Figs. 3 and 4 that the actual value of ϕ_{RecMin} approaches to 95° as a rectifier and ϕ_{InvMin} is around −103° as an inverter in the simulation. There exists the positive correlation relationship between the loss of MMC and S_{shadow}, if the MMC operates under the condition that the phase δ changes from 0 to 2π and the percentage "p" of I_{2m} to I_m is kept to be constant. And the differences are less than 10° between the calculated values and the actual value of the optimal phase of the SHCC component in the simulation.

Figs. 5 and 6 show that the loss of MMC and S_{shadow} decrease with the amplitude I_{2m} increasing from 0 to about $0.3I_m$ under the condition that the phase δ is set to be the optimal value. If the amplitude I_{2m} becomes greater than about $0.3I_m$, the loss of MMC increases rapidly while the S_{shadow} increases not obviously. Thereby, the actual value of the optimal I_{2m} is equal to about $0.3I_m$ in the computer simulation, that is if the MMC operates at the point $O_{\mathrm{p\_inject}}$ $(p = 30\%)$, the loss is minimum. During normal operation as a rectifier and an inverter, the amplitude I_m is about 1086 A under rated 1000 MW, and the dc component $|I_{\mathrm{dca}}|$ is around 476 A in the arm current. According to (17), the calculated value of the optimal I_{2m} is equal to 0.302 I_m, which has a good agreement with the simulation results. It is also seen from Figs. 5 and 6 that if the conventional method of eliminating the SHCC component is adopted, the MMC will operate at the point $O_{\mathrm{p\_eliminate}}$ where the loss is higher than the optimal point $O_{\mathrm{p\_inject}}$. Thus, the correctness of the analysis has been verified about the relationship between the amplitude I_{2m} and the loss of MMC and S_{shadow}.

III. Presented Loss Optimization Scheme

The SHCC component is caused by the mismatch between the phase arm voltage and the dc voltage. Different SHCC components can be injected into the arm current by adjusting the phase arm voltage. The proposed loss optimization scheme based on SHCC injection is shown in Fig. 7, which includes two parts: the generation of the optimal SHCC reference value and the injection of the optimal SHCC component. The control method based on the PR controller presented in [25] is used to inject the SHCC component into the arm current in this paper. And the LSF voltage balancing method in [8] is adopted to generate the switching pulse signals. In fact, the reference value i_{2f_ref} is set to be zero to eliminate the SHCC component of the arm current in the conventional loss optimization method, while the i_{2f_ref} is set to be the optimal value by the proposed loss optimization method in this paper. The analysis above shows that the loss of MMC has a good agreement with the S_{shadow}, but there still exist small differences between the actual values and the calculated values of the optimal phase and amplitude of the SHCC component. So, the loss optimization close-loop controller is designed to generate the optimal reference value i_{2f_ref} by minimizing the S_{shadow} under different operation conditions.

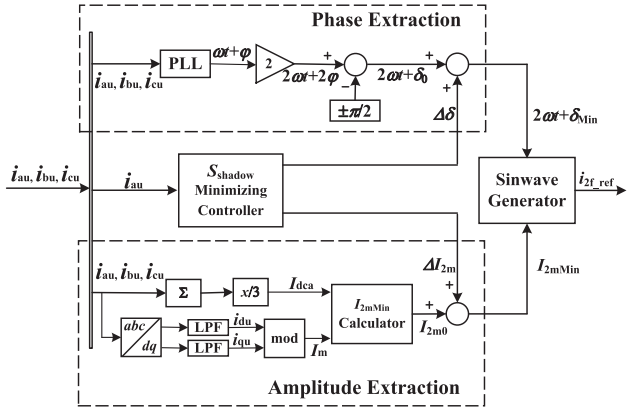

Fig. 8. Block diagram of the loss optimization closed-loop controller.

The loss optimization close-loop controller is shown in Fig. 8. The control cycle of the controller is the fundamental cycle T_f. In every control cycle T_f, the initial values of the optimal phase and amplitude are first extracted from the arm current i_{au}, i_{bu}, and i_{cu} according to (12), (14), and (17); then, the adjusting values $\Delta\delta$ and ΔI_{2m} are determined by the S_{shadow} minimizing controller; and at last, the optimal reference value i_{2f_ref} is generated by the optimal phase δ_{Min} and amplitude $I_{2m\mathrm{Min}}$ of the SHCC component. In the extraction of the initial phase, the phase of the fundamental component in arm current

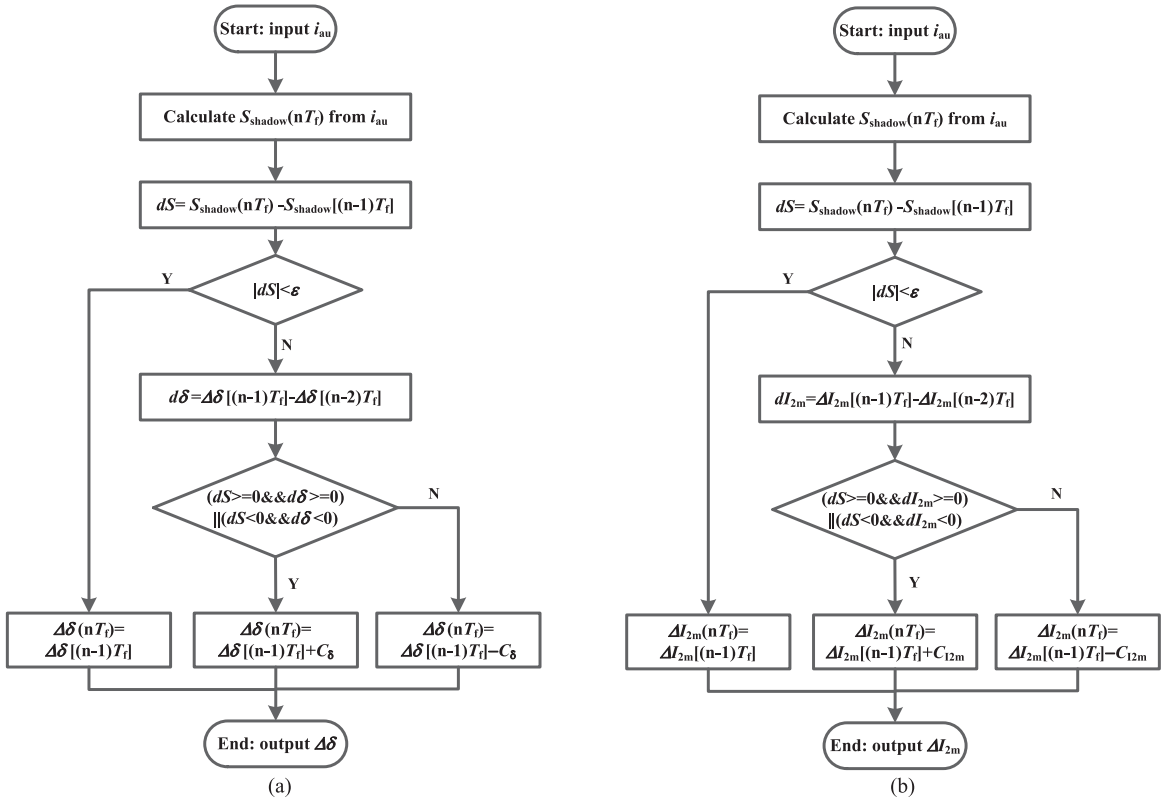

Fig. 9. Implementation method of the $S_{\rm shadow}$ minimizing controller.

is calculated as $\omega t + \varphi$ by the phase-locked loop method [29]. According to (12) and (14), the initial phase $2\omega t + \delta_0$ can be expressed by $2(\omega t + \varphi) + 0.5\pi$ as a rectifier and $2(\omega t + \varphi) - 0.5\pi$ as an inverter. The values of I_m and $I_{\rm dca}$ are necessary for calculating the initial value I_{2m0} from (17). $I_{\rm dca} = [i_{\rm au}(t) + i_{\rm bu}(t) + i_{\rm cu}(t)]/3$. The value of I_m is equal to the modulus of the $i_{\rm du}$ and $i_{\rm qu}$, i.e., $(i_{\rm du}^2 + i_{\rm qu}^2)^{0.5}$. The components $i_{\rm du}$ and $i_{\rm qu}$ in rotating frame are calculated by the Park transformation of the upper arm currents of three phases and loss-pass filters (LPFs). The cutoff frequency of the LPFs is 10 Hz.

The aim of the $S_{\rm shadow}$ minimizing controller is to modify the differences between the initial values and the optimal values of the δ and I_{2m} by the feedback of the arm current. The implementation process includes two steps. Step 1: under the assumption that ΔI_{2m} is equal to zero, the adjusting value $\Delta\delta$ can be determined by the method shown in Fig. 9(a). This method introduces the error dS of the $S_{\rm shadow}$ in the current control cycle $nT_{\rm f}$ and in the last control cycle $(n-1)T_f$ as the judgment condition of ending the adjustment of ΔI_{2m}. If $dS < \varepsilon$ ($\varepsilon = 0.01$ here), the current $\Delta\delta(nT_f)$ is the target value; else the error $d\delta$ of the $\Delta\delta[(n-1)T_f]$ and $\Delta\delta[(n-2)T_f]$ is also needed to be considered. If the $S_{\rm shadow}$ increases (dS>0) with the decreasing of the $\Delta\delta$ ($d\delta$ <0), or the $S_{\rm shadow}$ decreases (dS<0) with the increasing of the $\Delta\delta$ ($d\delta$ >0), the $\Delta\delta$ should be increased by C_δ ($C_\delta = 2^\circ \times \pi/180^\circ = 0.0349$) in the current control cycle. Else if the $S_{\rm shadow}$ increases ($dS >= 0$) with the increasing of the $\Delta\delta$ ($d\delta >= 0$), or the $S_{\rm shadow}$ decreases ($dS <= 0$) with the decreasing of the $\Delta\delta$ ($d\delta <= 0$), then the value of $\Delta\delta$ should be decreased by C_δ in the current control cycle. Step 2: when the adjustment of the value of $\Delta\delta$ has finished, the adjusting value ΔI_{2m} can be determined by the similar approach shown in Fig. 9(b), where $C_{I2m} = 5$ A.

IV. Simulation Results

In order to verify the performance of the proposed loss optimization method, computer simulations of ±350 kV/ 1000 MW MMC are carried out first in the time-domain simulation software PSCAD/EMTDC. The main circuit topology of the MMC is the same as Fig. 1 and the parameters are listed in Table I. The simulation results are shown in Figs. 10–15. In the simulation, the control scheme of eliminating the SHCC component or injecting the optimal SHCC component is adopted at $t = 2$ s. The calculation cycle of the $S_{\rm shadow}$ is $T_f = 0.02$ s and the calculation cycle of the loss of MMC is $5T_f = 0.1$ s. Thus, the waves of the $S_{\rm shadow}$ and the loss of MMC $P_{\rm loss}$ lag behind the upper arm current $i_{\rm armU}$.

Figs. 10 and 11 demonstrate the simulation results as a rectifier under rated 1000 MW by adopting the conventional method of eliminating the SHCC component and the proposed control scheme based on the optimal SHCC component injection. Comparing the two figures, it is seen that the fluctuation of the SM voltage $u_{\rm smAU}$ is reduced from 295 V (1780 V–1485 V) to 194 V (1714 V–1520 V) by injecting the optimal SHCC component and 248 V (1752 V–1504 V) by eliminating the SHCC component. The response time of the $S_{\rm shadow}$ minimizing controller in the proposed control scheme is less than 0.1 s. And the loss $P_{\rm loss}$ is reduced by around 0.94 MW, i.e., $13.4\% = (7.01\ {\rm MW} - 6.07\ {\rm MW})/\ 7.01\ {\rm MW}$, with the proposed control scheme as a rectifier under rated power, whereas the

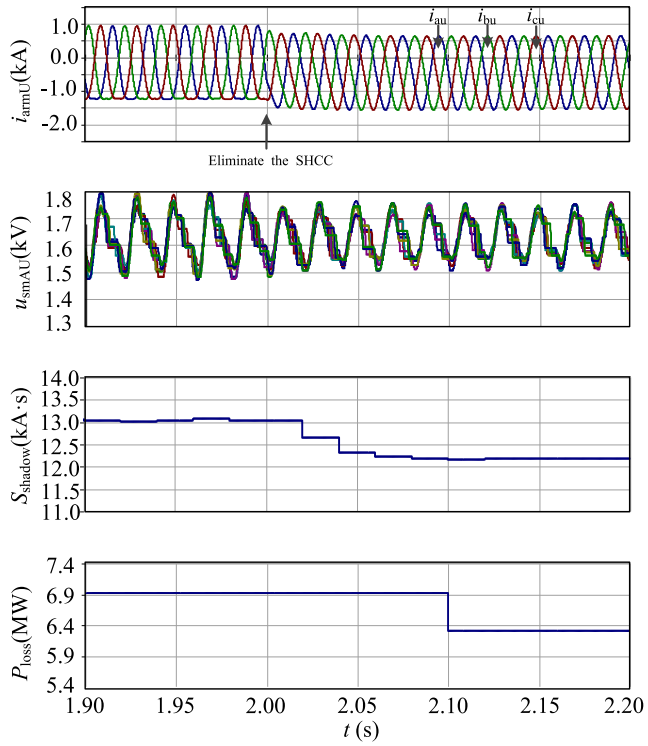

Fig. 10. Simulation results of eliminating the SHCC component at $t = 2$ s as a rectifier under rated 1000 MW.

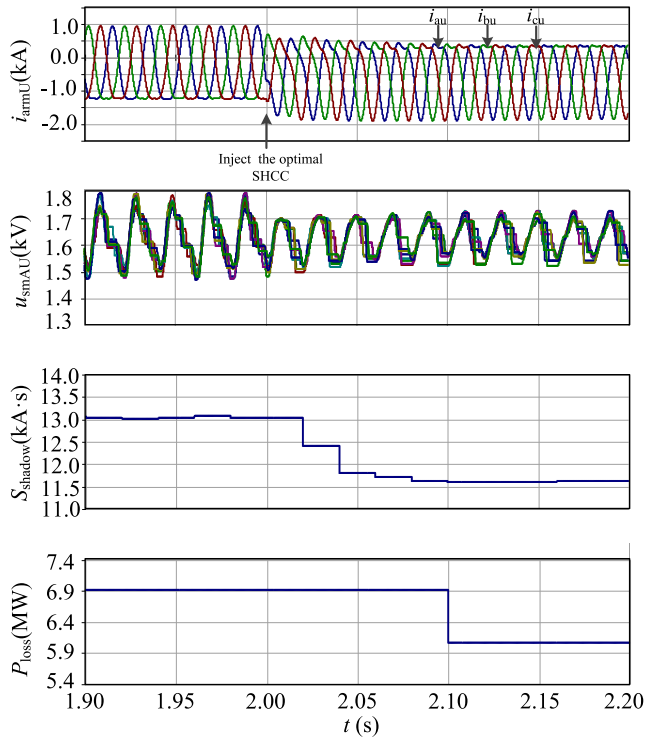

Fig. 11. Simulation results of injecting the optimal SHCC component at $t = 2$ s as a rectifier under rated 1000 MW.

$P_{\rm loss}$ is reduced by about 0.66 MW, i.e., $9.4\% = (7.01\ \text{MW} - 6.35\ \text{MW})/\ 7.01\ \text{MW}$, with the conventional method.

From the simulation results shown in Figs. 12 and 13, it is clear that the fluctuation of the SM voltage $u_{\rm smAU}$

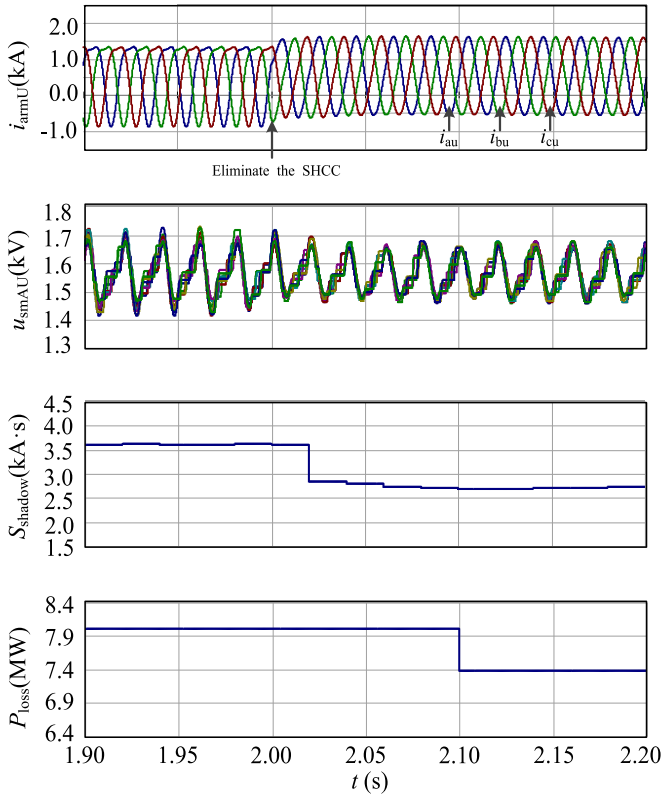

Fig. 12. Simulation results of eliminating the SHCC component at $t = 2$ s as an inverter under rated 1000 MW.

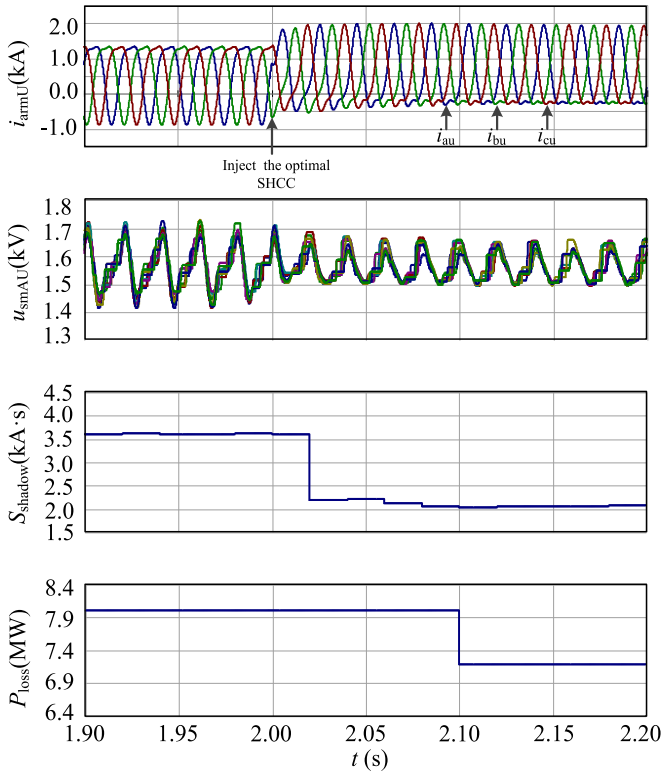

Fig. 13. Simulation results of injecting the optimal SHCC component at $t = 2$ s as an inverter under rated 1000 MW.

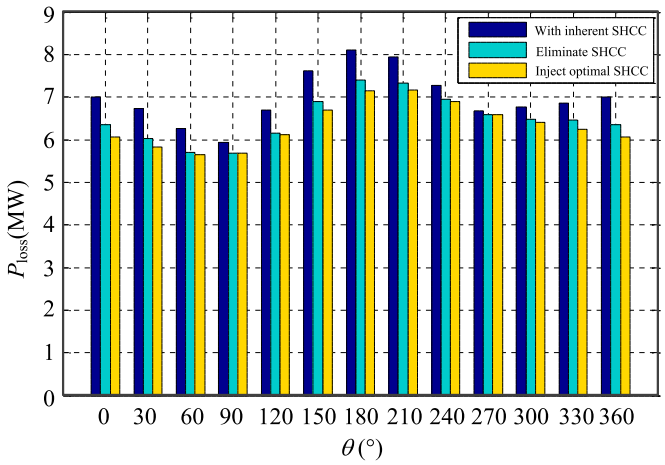

Fig. 14. Histogram of the loss calculated under different power factor angles when the apparent power of MMC $S = 1000$ MVA with three different control schemes.

is reduced from 302 V (1712 V–1410 V) to 213 V (1685 V–1472 V) by adopting the conventional method if the MMC operates as an inverter under rated 1000 MW. And the loss $P_{\rm loss}$ of MMC is reduced by about 0.69 MW, i.e., $8.5\% = (8.10\,\text{MW} - 7.41\,\text{MW})/\,8.10\,\text{MW}$, with the conventional method. Comparing with the performance of the conventional method, the fluctuation of the SM voltage is reduced from 302 V to 170 V (1668 V–1498 V), the response time of the $S_{\rm shadow}$ minimizing controller is less than 0.1 s, and the loss $P_{\rm loss}$ is reduced by around 0.96 MW, i.e., $11.9\% = (8.10\,\text{MW} - 7.14\,\text{MW})/\,8.10\,\text{MW}$, with the proposed control scheme as an inverter under rated power.

The simulation results of the loss of MMC have been compared under different power factor angles with three control schemes in Fig. 14. The first control scheme is that the MMC operates normally with the inherent SHCC component, the second scheme is the conventional method of eliminating the SHCC component, and the third scheme is the proposed loss optimization method based on injecting the optimal SHCC component. The phase of the ac grid voltage is taken as the reference value in this paper, so the power factor angle θ is equal to $\varphi \times 180°/\pi$. When the MMC outputs apparent power $S = 1000\,\text{MVA}$ to the ac side grid, the loss of MMC can be reduced by both the second and third control schemes under different power factor angles. According to Fig. 14, it is clear that if the MMC operates at $\theta = 90°$ or $\theta = 270°$, $I_{\rm dca} = 0$, and the optimal I_{2m} is equal to 0.0043 I_m from (17). The optimal operation point $O_{\rm p\_inject}$ is very near to the point $O_{\rm p\_eliminate}$ $(I_{2m} = 0I_m)$, so the performance of the proposed scheme is better but not much than the conventional method at $\theta = 90°$ or $\theta = 270°$. The advantage of the presented method becomes more and more apparent with the increase of the active power of the MMC, and the performance of the proposed scheme is best at $\theta = 0°$ or $\theta = 180°$, that is, the output active power reaches the rated power.

The SM fault is one of the common faults of MMC. Redundant SMs are set to improve the reliability and performance of MMC. If the number of the fault SMs is less than $N_{\rm fN}$, MMC

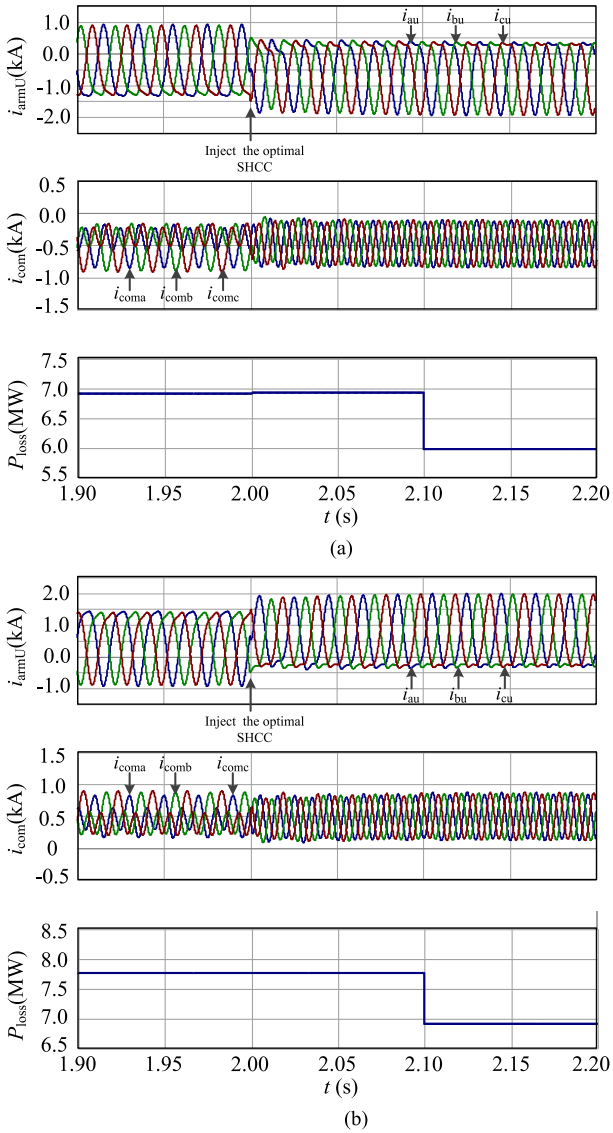

Fig. 15. Simulation results of injecting the optimal SHCC component at $t = 2$ s under the SMs' fault conditions. (a) Rectifier. (b) Inverter.

can operate normally but the fundamental fluctuation will be induced in the dc component of the arm current [30]. So, it is necessary to study the performance of the proposed scheme under the SM fault conditions. Take a typical fault condition for example, that is, $N_{\rm fN} = 30$ SMs break down on the upper arm of phase A, the lower arms of phase B and C respectively, the simulation results are shown in Fig. 15. It is clear from the arm currents $i_{\rm armU}$ and the common mode components $i_{\rm com}$ that the optimal SHCC can be injected into the arm current by the proposed scheme under the SM fault conditions. And the power loss of MMC is reduced by about 0.96 MW as a rectifier and about 0.95 MW as an inverter by adopting the loss optimization method under the fault conditions. Therefore, the correctness of the proposed scheme is verified under the SM fault conditions.

V. Experimental Verification

In order to verify the correctness of the presented loss optimization method in Section III and the analysis in Section IV

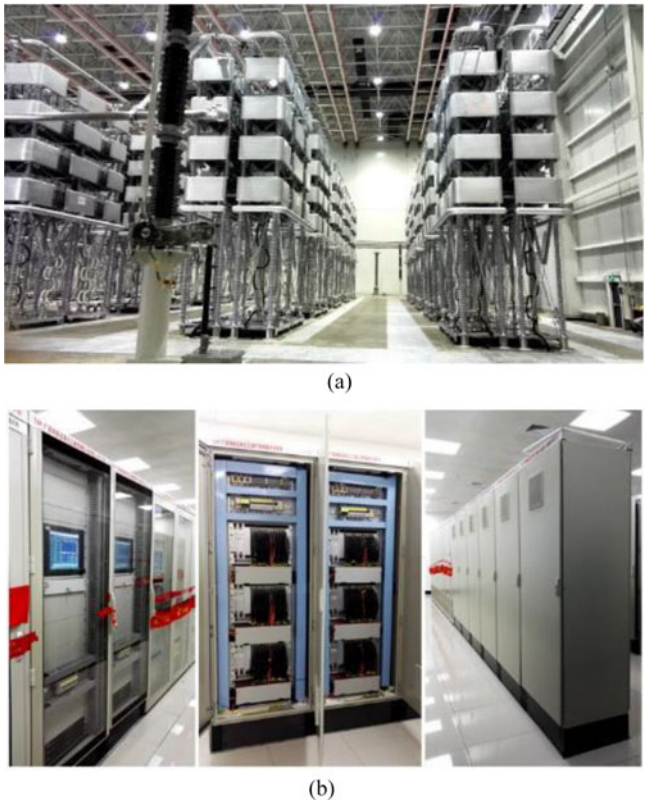

Fig. 16. Valve tower of the Guangxi side MMC at Luxi HVdc Project site. (a) MMC valve. (b) Valve control and protection system.

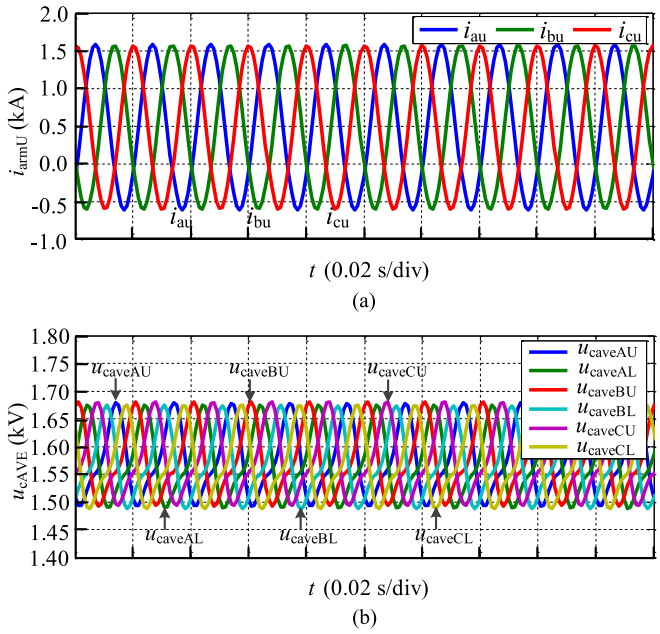

Fig. 17. Experimental results of the Guangxi side MMC under rated 1000 MW. (a) Upper arm current. (b) SMs' average voltage of six arms of MMC.

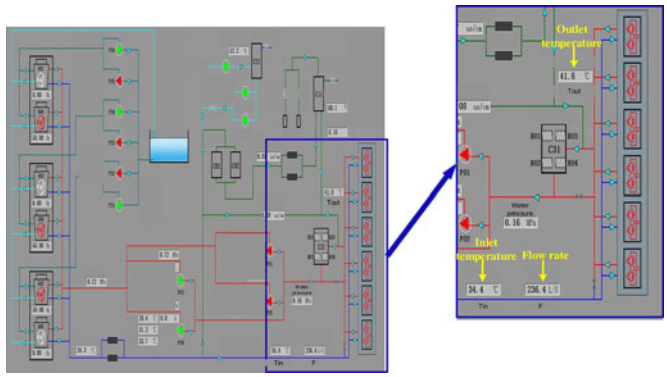

Fig. 18. Experimental results of the water cooling system for the Guangxi side MMC valve at Luxi HVdc Project site.

further, the experiments and the HIL tests have been carried out. The accuracy of the simulation look-up table method [9]–[11] is tested by the experimental results of the MMC at the project site. The presented loss optimization method is verified by the results of the HIL tests and a down-scaled MMC setup. The main circuit topology of the MMC is the same as Fig. 1 in the HIL tests and the experiments at the project site. The parameters are listed in Table I.

A. *Experimental Results at the Project Site*

The calculation of the loss of MMC is mainly based on the simulation look-up table method in this paper. The accuracy of the simulation look-up table method is vital for the analysis of the proposed loss optimization method. So, the experiments are carried out to verify the accuracy of the simulation look-up table method at the Luxi Back-to-Back DC Asynchronous Networking Project site [28]. This project is used to connect the Yunnan Power Grid and CSG Main Grid. The two-side MMCs of the VSC-HVdc unit are the Yunnan side MMC as a rectifier and the Guangxi side MMC as an inverter in this project. The topology and the system parameters of the Guangxi side MMC are the same as those in the simulation. Fig. 16 shows the valve and the control and protection system of the Guangxi side MMC.

The water cooling system is installed on the MMC valve tower to take away the heat produced by the IGBT modules in SMs. The loss of MMC, which mainly refers to the loss of IGBTs and diodes in the SMs in this paper, can be calculated by the data of the water cooling system in thermal equilibrium. The data include the inlet water temperature of the water cooling system $T_{\rm in}(^\circ{\rm C})$, the outlet water temperature $T_{\rm out}(^\circ{\rm C})$, the flow rate F(L/s), the specific heat capacity of the water $c = 4200\,{\rm J}/({\rm kg}\cdot^\circ{\rm C})$, and the density of the water $\rho_{\rm water} = 1\,{\rm kg/L}$. Although the water cooling system contacts with the substrate of IGBT module directly, it cannot take away the total heat. There is about 5% of the heat dissipating into air, which is measured by the manufacturer of the water cooling system at the project site. So, the water cooling system takes away 95% of the heat produced by the MMC.

Due to the limit of the operation regulation, the data of the Guangxi side MMC is available under the condition that the MMC operates with the control method of eliminating the SHCC component as an inverter. The upper arm current and the SM's average voltage are given in Fig. 17 under rated 1000 MW. Fig. 18 shows the data of the water cooling system in thermal equilibrium. $T_{\rm in} = 34.4\,^\circ{\rm C}$,

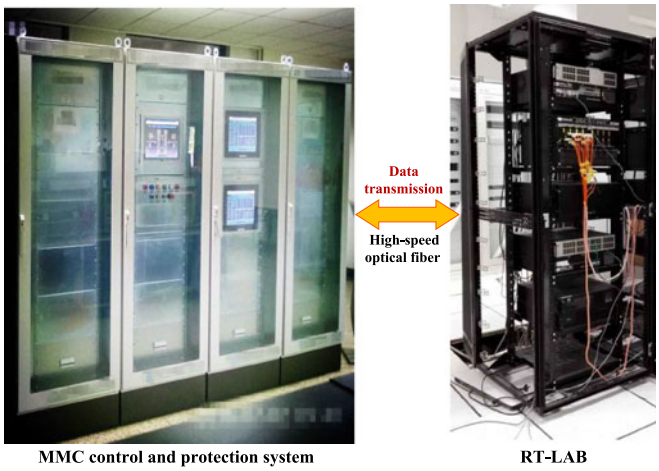

Fig. 19. HIL test platform based on the RT-LAB (OP7000) and the MMC control and protection system.

$T_{\text{out}} = 41.8\,^{\circ}\text{C}$, and $F = 236.4$ L/s. The loss of MMC can be calculated as $P_{\text{loss}} = (T_{\text{out}} - T_{\text{in}})Fc\rho_{\text{water}}/95\% = (41.8\,^{\circ}\text{C} - 34.4\,^{\circ}\text{C}) \times 236.4\,\text{L/s} \times 4200\,\text{J/(kg}\cdot^{\circ}\text{C)} \times 1\,\text{kg/L}/95\% = 7.73$ MW. The value of the loss is 7.41 MW calculated by the simulation look-up table method. The calculation error of the method is about $(7.73 - 7.41)/7.73 \times 100\% = 4.1\%$. Hence, the simulation look-up table method has high accuracy in calculating the loss of MMC.

B. HIL Test

The correctness of the proposed scheme has been proved in the computer simulation above. However, the control and protection system at the project site is greatly different from the computer simulation in the generation and transmission process of the switching signals of all SMs. It imposes high requirements on the design of the presented controller. So, the effectiveness of the proposed method still needs to be verified further in the control system at the project site. In this section, the proposed loss optimization scheme is verified on the RT-LAB (OP7000) based HIL test platform. The MMC control and protection system and the RT-LAB (OP7000) are shown in Fig. 19. The main circuit of MMC is built in the RT-LAB (OP7000). The HIL test platform has the same topology, parameters, control methods, and the control and protection system as the experiments at project site. Additionally, the proposed optimization scheme and the calculation of the loss of MMC are implemented in the MMC control and protection system of the HIL test platform as well. The loss of MMC is calculated by the simulation look-up table method. The exchanged data, such as the switching signals, the voltage, and state of the SMs, are transmitted by the high-speed optimal fiber between the RT-LAB (OP7000) and the MMC control and protection system.

Figs. 20 and 21 show the HIL test results of the proposed loss optimization scheme. It is seen from Fig. 20 that if the MMC operates as a rectifier under rated 1000 MW, the loss of MMC P_{loss} reduces to about 6.45 MW and the S_{shadow} reduces to 12.5 kA·s by adopting the conventional method to eliminate the SHCC component; the loss P_{loss} reduces to about 6.15 MW,

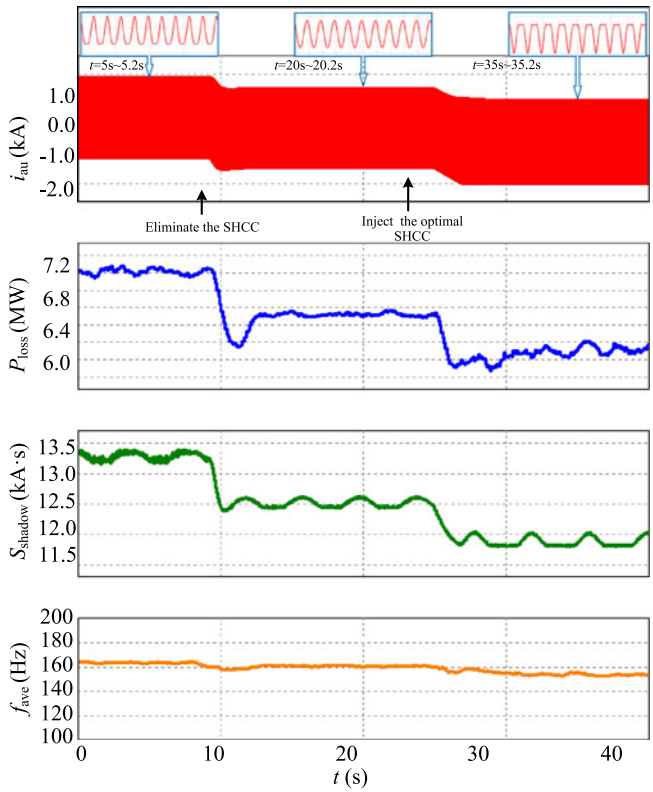

Fig. 20. HIL test results of adopting the proposed loss optimization scheme as a rectifier under rated 1000 MW.

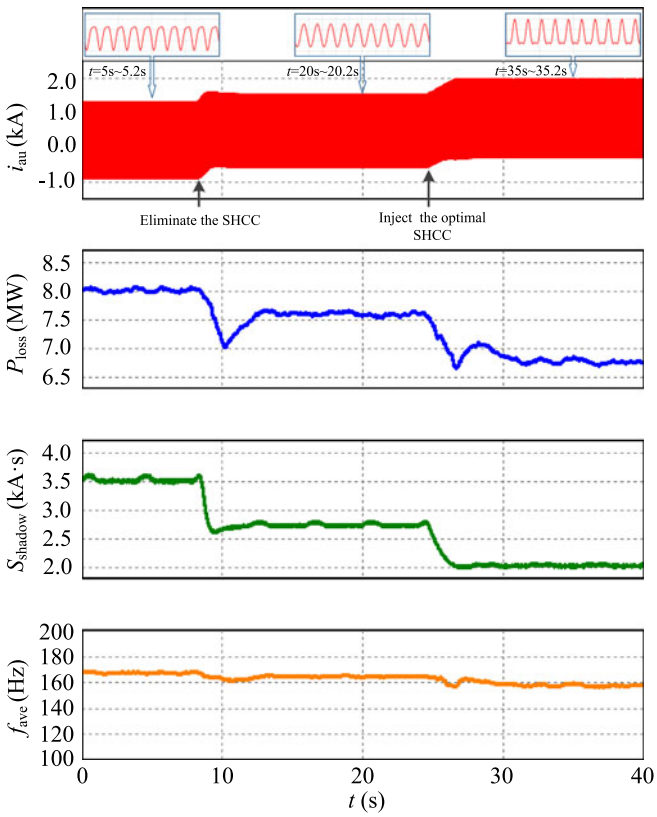

Fig. 21. HIL test results of adopting the proposed loss optimization scheme as an inverter under rated 1000 MW.

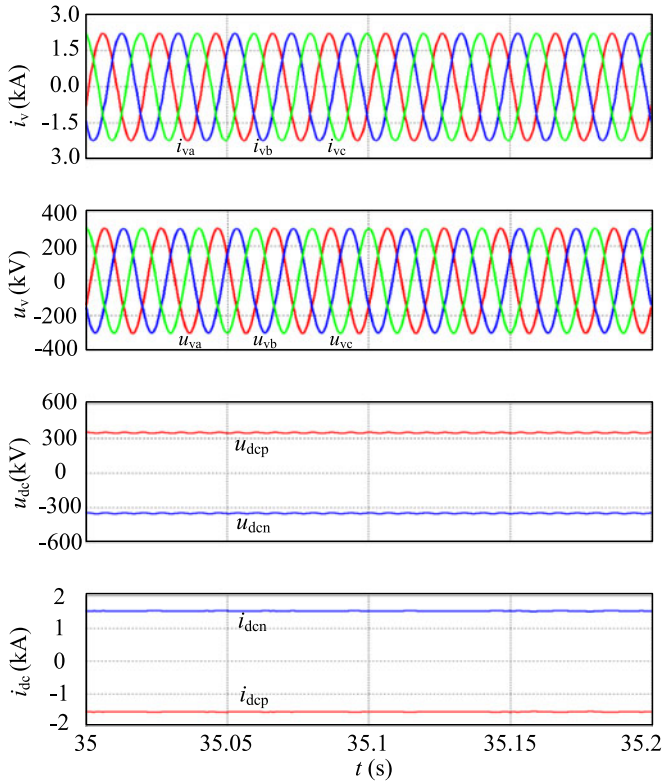

Fig. 22. Output current and voltage in the grid and dc side as a rectifier under rated 1000 MW during $t = 35 - 35.2$ s.

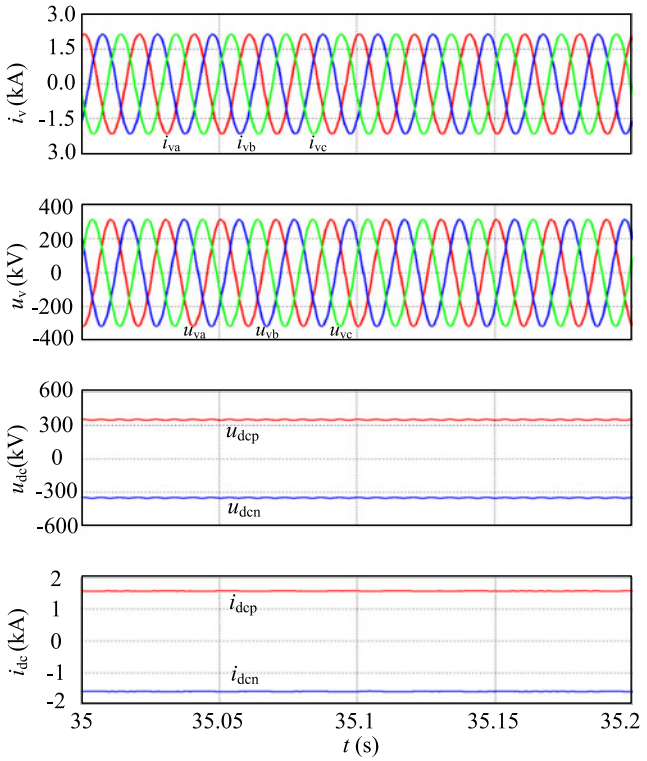

Fig. 23. Output current and voltage in the grid and dc side as an inverter under rated 1000 MW during $t = 35 - 35.2$ s.

the $S_{\rm shadow}$ reduces to 11.8 kA·s, and the average frequency $f_{\rm ave}$ of the SMs decreases by about 10 Hz by the presented loss optimization method based on injecting the optimal SHCC component. If the MMC operates as an inverter under rated 1000 MW, Fig. 21 shows that the loss of MMC $P_{\rm loss}$ reduces to about 7.54 MW and the $S_{\rm shadow}$ reduces to 2.8 kA·s by using the conventional method; the average frequency $f_{\rm ave}$ of the SMs can be reduced by about 10 Hz, the loss $P_{\rm loss}$ can be reduced to about 6.85 MW, and the $S_{\rm shadow}$ reduces to 2.0 kA·s by the presented loss optimization method. Compared with the simulation results in Section IV, the calculation errors of the loss in the HIL test are less than 5%. It is seen from Figs. 22 and 23 that the output ac current, the ac voltage, the dc voltage and current are not affected by the injection of the optimal SHCC component. Thus, the results of the HIL test prove that the presented method has better performance than the conventional method in reducing the loss of MMC. Meanwhile, the results also verify the effectiveness of the proposed loss optimization controller in the engineering application.

C. Experimental Results of a Down-Scaled MMC Setup

The proposed loss optimization control scheme is verified on a down-scaled MMC setup as well. Fig. 24 shows the main circuit of the MMC setup, where a diode rectifier is connected to the ac grid of 380 V and the MMC inverter is connected to the resistance load $R_L = 2.5\,\Omega$. The MMC consists of six arms, each formed by two series-connected SMs and one arm inductor $L_{\rm arm} = 4$ mH. The rated dc voltage is 200 V, the rated SM capacitor voltage is 100 V, the capacitance of SM is 6.72 mF, and the capacitance of C_1 is 5.4 mF. The photographs of the MMC setup are shown in Fig. 25.

The IGBT module used in the MMC setup is Infineon F475R06W1E3, in which there is an inner thermistor R_t. In order to measure the inner temperature of the IGBT module by using the thermistor R_t, the measuring circuit is designed in the SM board, as shown in Fig. 25. The value of the voltage V_t can be obtained by the monitor system, then the value of R_t is equal to $V_t R_t/(5 - V_t)$. According to the thermistor temperature characteristic $T = f(R_t)$ in the datasheet of Infineon F475R06W1E3, the inner temperature of IGBT can be measured before and after the proposed loss optimization control scheme is adopted. The experimental results are shown in Figs. 26 and 27.

Fig. 26 illustrates the waveforms of the arm current $i_{\rm au}$, $i_{\rm al}$, and the output voltage $u_{\rm v\_ab}$, $u_{\rm v\_bc}$ of the MMC setup before and after the presented control scheme is adopted. From Fig. 26(a), it is clear that the amplitude of the inherent SHCC component is near to zero, which is resulted from the parameters of SMs' capacitor and the arm inductor. The peak value of the $u_{\rm v\_ab}$ is around 138 V, so the MMC output power is about 3.84 kW in the experiment. It is also seen that the optimal SHCC component can be injected into the arm current by the proposed method without the current surge. And the output voltage is not affected by the proposed method. Thus, the controller of loss optimization has a good performance when injecting the optimal SHCC component.

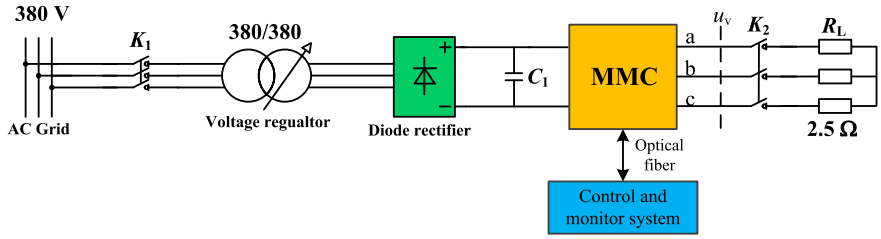

Fig. 24. Main circuit of the down-scaled MMC setup.

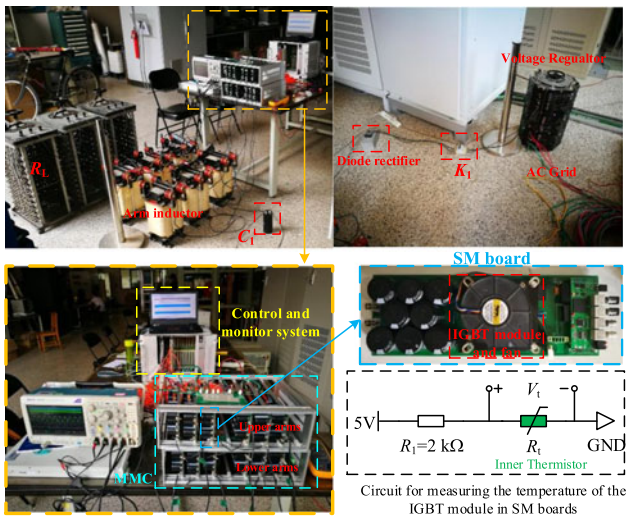

Fig. 25. Photographs of the MMC setup.

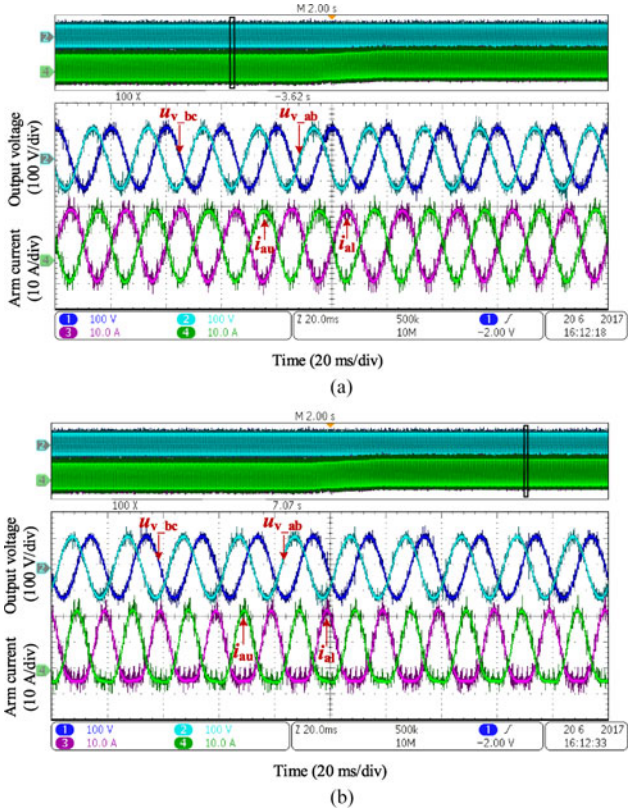

Fig. 26. Arm current i_{au}, i_{al} and the output voltage $u_{\mathrm{v\_ab}}$, $u_{\mathrm{v\_bc}}$ of the MMC setup. (a) Before the proposed control scheme is adopted. (b) After the proposed control scheme is adopted.

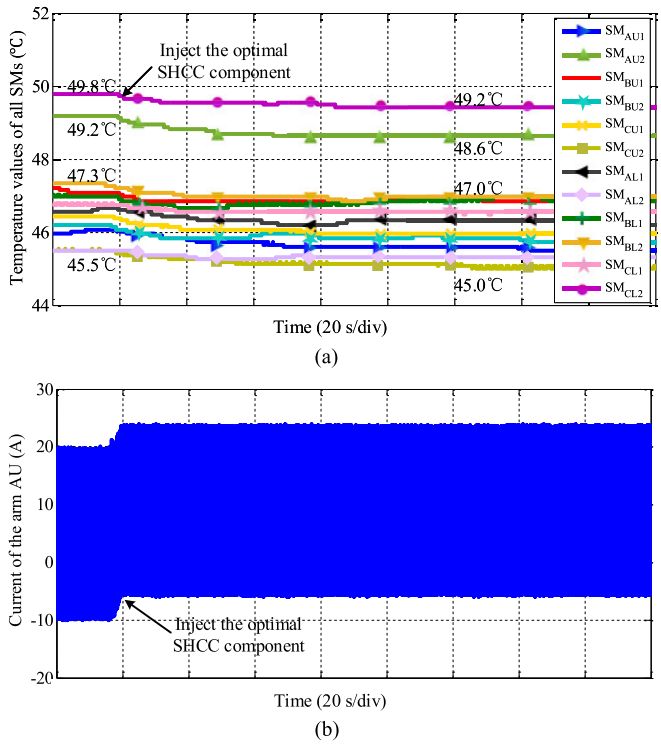

Fig. 27. Experimental results in the MMC setup: (a) temperature values of all SMs; and (b) current waveform of the arm AU.

Fig. 27 indicates the temperature waveforms of all SMs and the current waveform of the arm AU when the optimal SHCC component is injected into the arm current. From Fig. 27(a), the maximum temperature value of all SMs is 49.8 °C, and the minimum value is 45.5 °C when the MMC is in the thermal equilibrium state before the presented loss optimization control scheme is adopted. After the optimal SHCC component is injected into the arm current, the maximum and minimum temperature values are reduced to 49.2 and 45.0 °C, respectively in the thermal equilibrium state. The temperature of every SM is reduced by 0.4 °C averagely when using the proposed loss optimization control scheme. Thus, the experimental results of the down-scaled MMC setup verify the effectiveness of the proposed loss optimization control scheme based on the optimal SHCC injection.

VI. Conclusion

In this paper, the analysis on the relationship between the loss and the arm current of MMC demonstrates that the loss

and the negative area $S_{\rm shadow}$ of the arm current are positively correlated. The optimal values of the phase and amplitude of the SHCC component are derived by minimizing the $S_{\rm shadow}$, whereas the optimal value of the amplitude is not zero. A loss optimization control scheme is also proposed by injecting the optimal SHCC component into the arm current of MMC. The effectiveness and correctness of the proposed method are verified by the computer simulation, the HIL test, and a down-scaled MMC setup. The simulation and HIL test results show better performance over the conventional method of eliminating the SHCC component in terms of reducing the loss of MMC. It is also observed that the loss of MMC can be reduced by around 10% by adopting the presented method under rated 1000 MW in comparison with the operation condition with the inherent SHCC component. The experimental results of the down-scaled MMC setup illustrate that the temperature of all SMs can be reduced by adopting the proposed loss optimization control scheme.

ACKNOWLEDGMENT

The authors would like to express heartfelt thanks to the China Southern Power Grid Company, Ltd., and the Xi'an XD Power Systems Company, Ltd. for providing help to finish the experiments at the Luxi Back-to-Back DC Asynchronous Networking Project site for this paper.

REFERENCES

[1] A. Lesnicar and R. Marquardt, "An innovative modular multilevel converter topology suitable for a wide power range," in *Proc. IEEE Power Tech. Conf.*, Bologna, Italy, 2003, pp. 1–6.

[2] N. Flourentzou, V. G. Agelidis, and G. D. Demetriades, "VSC-based HVDC power transmission systems: An overview," *IEEE Trans. Power Electron.*, vol. 24, no. 3, pp. 592–602, Mar. 2009.

[3] S. Debnath, J. Qin, B. Bahrani, M. Saeedifard, and P. Barbosa, "Operation, control, and applications of the modular multilevel converter: A review," *IEEE Trans. Power Electron.*, vol. 30, no. 1, pp. 37–53, Jan. 2015.

[4] A. Nami, J. Liang, F. Dijkhuizen, and G. D. Demetriades, "Modular multilevel converters for HVDC applications: Review on converter cells and functionalities," *IEEE Trans. Power Electron.*, vol. 30, no. 1, pp. 18–36, Jan. 2015.

[5] M. A. Perez, S. Bernet, J. Rodriguez, S. Kouro, and R. Lizana, "Circuit topologies, modeling, control schemes, and applications of modular multilevel converters," *IEEE Trans. Power Electron.*, vol. 30, no. 1, pp. 4–17, Jan. 2015.

[6] J. Peralta, H. Saad, S. Dennetière, J. Mahseredjian, and S. Nguefeu, "Detailed and averaged models for a 401-level MMC-HVDC system," *IEEE Trans. Power Del.*, vol. 27, no. 3, pp. 1501–1508, Jul. 2012.

[7] S. Rohner, S. Bernet, M. Hiller, and R. Sommer, "Modulation, losses, and semiconductor requirements of modular multilevel converters," *IEEE Trans. Ind. Electron.*, vol. 57, no. 8, pp. 2633–2642, Aug. 2010.

[8] Z. Li *et al.*, "Power module capacitor voltage balancing method for a ±350-kV/1000-MW modular multilevel converter," *IEEE Trans. Power Electron.*, vol. 31, no. 6, pp. 3977–3984, Jun. 2016.

[9] S. Rodrigues, A. Papadopoulos, E. Kontos, T. Todorcevic, and P. Bauer, "Steady-state loss model of half-bridge modular multilevel converters," *IEEE Trans. Ind. Appl.*, vol. 52, no. 3, pp. 2415–2425, May 2016.

[10] H. Wang *et al.*, "Power loss and junction temperature analysis in the modular multilevel converters for HVDC transmission systems," *J. Power Electron.*, vol. 15, no. 3, pp. 685–694, May 2015.

[11] Z. Zhang, Z. Xu, and Y. Xue, "Valve loss calculation of MMC-HVDC based on piecewise analytical formula," *Autom. Elect. Power Syst.*, vol. 37, no. 15, pp. 109–116+151, Aug. 2013.

[12] M. Zygmanowski, B. Grzesik, M. Fulczyk, and R. Nalepa, "Analytical and numerical power loss analysis in modular multilevel converter," in *Proc. 2013 39th Annu. Conf. IEEE Ind. Electron. Soc.*, Vienna, Austria, 2013, pp. 465–470.

[13] L. Yang, Y. Li, Z. Li, P. Wang, F. Gao, and F. Xu, "A simplified loss model of modular multilevel converter," in *Proc. 2016 IEEE PES Asia–Pac. Power Energy Eng. Conf.*, Xi'an, China, 2016, pp. 661–665.

[14] L. Qiang, P. Hui, and H. Zhiyuan, "Analytic calculation method for loss and junction temperature of modular multilevel converter," *Autom. Elect. Power Syst.*, vol. 40, no. 4, pp. 85–91, Feb. 2016.

[15] S. Huang *et al.*, "Analysis and calculation on switching frequency and switching losses of modular multilevel converter with maximum submodule capacitor voltage deviation," *IET Power Electron.*, vol. 9, no. 2, pp. 188–197, Oct. 2016.

[16] Y. Li, E. A. Jones, and F. F. Wang, "The impact of voltage-balancing control on switching frequency of the modular multilevel converter," *IEEE Trans. Power Electron.*, vol. 31, no. 4, pp. 2829–2839, Apr. 2016.

[17] M. Saeeidifard and R. Iravani, "Dynamic performance of a modular multilevel back-to-back HVDC system," *IEEE Trans. Power Del.*, vol. 25, no. 4, pp. 2903–2912, Oct. 2010.

[18] H. Peng, M. Hagiwara, and H. Akagi, "Modeling and analysis of switching-ripple voltage on the DC link between a diode rectifier and a modular multilevel cascade inverter (MMCI)," *IEEE Trans. Power Electron.*, vol. 28, no. 1, pp. 75–84, Jan. 2013.

[19] Q. Tu, Z. Xu, and L. Xu, "Reduced switching-frequency modulation and circulating current suppression for modular multilevel converters," *IEEE Trans. Power Del.*, vol. 26, no. 3, pp. 2009–2017, Jul. 2011.

[20] P. M. Meshram and V. B. Borghate, "A simplified nearest level control (NLC) voltage balancing method for modular multilevel converter (MMC)," *IEEE Trans. Power Electron.*, vol. 30, no. 1, pp. 450–462, Jan. 2015.

[21] W. Zhou *et al.*, "Common-mode voltage injection-based nearest level modulation with loss reduction for modular multilevel converters," *IET Renewable Power Gener.*, vol. 10, no. 6, pp. 798–806, Feb. 2016.

[22] J. Qin and M. Saeedifard, "Reduced switching-frequency voltage-balancing strategies for modular multilevel HVDC converters," *IEEE Trans. Power Del.*, vol. 28, no. 4, pp. 2403–2410, Oct. 2013.

[23] F. Erturk and A. M. Hava, "A detailed power loss analysis of modular multilevel converter," in *Proc. 2015 IEEE Appl. Power Electron. Conf. Expo.*, Charlotte, NC, USA, 2015, pp. 1658–1665.

[24] R. Hong *et al.*, "Loss calculation method and characteristics analysis for MMC-HVDC system," *Elect. Power Autom. Equip.*, vol. 6, pp. 101–106, Jun. 2014.

[25] Z. Li, P. Wang, Z. Chu, H. Zhu, Y. Luo, and Y. Li, "An inner current suppressing method for modular multilevel converters," *IEEE Trans. Power Electron.*, vol. 28, no. 11, pp. 4873–4879, Nov. 2013.

[26] L. Yang, Y. Li, Z. Li, and P. Wang, "Efficiency optimization of MMC adopting harmonic circulating current injection," in *Proc. 2016 42nd Annu. Conf. IEEE Ind. Electron. Soc.*, Florence, Italy, 2016, pp. 2557–2562.

[27] J. Pou, S. Ceballos, G. Konstantinou, V. G. Agelidis, R. Picas, and J. Zaragoza, "Circulating current injection methods based on instantaneous information for the modular multilevel converter," *IEEE Trans. Ind. Electron.*, vol. 62, no. 2, pp. 777–788, Feb. 2015.

[28] China Southern Power Grid, Guangzhou, China, Press Release, Aug. 29, 2016. [Online]. Available: http://eng.csg.cn/Press_release/News_2016/201609/t2016 0905_142899.html

[29] S. Golestan, M. Ramezani, J. M. Guerrero, and M. Monfared, "dq-frame cascaded delayed signal cancellation-based PLL: Analysis, design, and comparison with moving average filter-based PLL," *IEEE Trans. Power Electron.*, vol. 30, no. 3, pp. 1618–1632, Mar. 2015.

[30] P. Hu, D. Jiang, Y. Zhou, Y. Liang, J. Guo, and Z. Lin, "Energy balancing control strategy for modular multilevel converters under submodule fault conditions," *IEEE Trans. Power Electron.*, vol. 29, no. 9, pp. 5021–5030, Sep. 2014.

Limin Yang was born in Shanxi Province, China, in 1991. He received the B.S. degree in electrical engineering from Tianjin University, Tianjin, China, in 2012. Since September 2012, he has been working toward the Ph.D. degree in power electronics and power drives from the Institute of Electrical Engineering, Chinese Academy of Sciences, Beijing, China.

His research interests include loss analysis and control of modular multilevel converter, especially its applications in high-voltage direct-current fields.

Yaohua Li was born in Henan, China, in 1966. He received the Ph.D. degree in power electronics and power drives from Tsinghua University, Beijing, China, in 1994.

From 1995 to 1997, he was a Postdoctoral Research Fellow in the Institute of Electrical Machine, Technical University of Berlin, Berlin, Germany. In 1997, he joined the Institute of Electrical Engineering, Chinese Academy of Sciences, Beijing, China, where he is currently a Professor and Vice Director. His research interests include analysis and control of electrical machines, power electronics, etc.

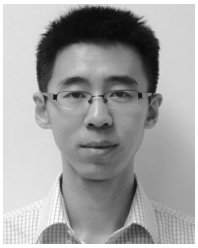

Zixin Li (S'08–M'10–SM'16) was born in Hebei Province, China, in 1981. He received the B.Eng. degree in industry automation from North China University of Technology, Beijing, China, in 2001, and the Ph.D. degree (with Hons.) in power electronics and power drives from the Institute of Electrical Engineering, Chinese Academy of Sciences, Beijing, China, in 2010.

In 2010, he joined the Institute of Electrical Engineering, Chinese Academy of Sciences, where he is currently a Professor. He has authored and coauthored more than 60 academic papers and holds five invention patents in China. His research interests include circuit topology, control and analysis of power converters, especially multilevel converters in high-power fields.

Dr. Li is an Associate Editor of the IEEE TRANSACTIONS ON POWER ELECTRONICS. He received many honors and awards from IEEE and the government. He was the winner of IEEE Power Electronics Society Richard M. Bass Outstanding Young Power Electronics Engineer Award of 2015 for his contributions to multilevel and HVdc converters.

Ping Wang was born in Shanghai, China, in 1955. He received the B.S. degree in computer science from Lanzhou University, Lanzhou, China, in 1980.

Since 1980, he has been with the Institute of Electrical Engineering, Chinese Academy of Sciences, Beijing, China, where became an Assistant Engineer in 1985, a Senior Engineer in 1993, and a Professor of power electronics and power drives in 2008. From 1995 to 1996, he was a Visiting Researcher with the Fraunhofer Institute for Production Systems and Design Technology, Berlin, Germany. His research interests include power electronics, static power converters, active filter, ac drives, etc.

Prof. Wang is a member of the China Electrotechnical Society.

Shukai Xu was born in Guangdong, China, in 1978. He received the B.E.E. and Ph.D. degrees from Tsinghua University, Beijing, China, in 2002 and 2007, respectively, both in electrical engineering.

He is currently a Professor of engineering in Electric Power Research Institute, China Southern Power Grid, Guangzhou, China. His research interests include FACTS and VSC-HVdc.

Ruifeng Gou was born in Shaanxi Province in 1959. He received the B.S. degree in electrical engineering from Xi'an Jiaotong University, China, in 1982.

He has been working in the development of power equipment for more than 30 years. He is currently the Vice Chief Engineer of China XD Group Company, Ltd., Xi'an, China. He is also a Senior Expert in the electrical engineering, and has extensive research and project experience in the equipment development and test technology. He led the key technology research and equipment development of the first 4000 and 5100 A direct current transfer switch, the first $\pm$160 kV/50 MW, $\pm$350 kV/1000 MW, $\pm$800 kV/5000 MW VSC-HVdc converters, and the first 6250 A and 1100 kV LCC-HVdc converters in China. He led to establish the standard system of dc equipment in China.

Mr. Gou received the first prize of National Science and Technology Progress Award in 2009, the first China Mechanical Industry Science and Technology Awards in 2007, 2010, 2013, and 2015, and the first China Electrical Power Science and Technology Award in 2013.